Concentration and Temperature Dependence of Dynamic Light Scattering for Some Polystyrene Solutions in Toluene, Cyclohexane, Methylcyclohexane and Deuteromethylcyclohexane

Jerzy Szydlowski[†] and W. Alexander Van Hook*

Chemistry Department, University of Tennessee, Knoxville, Tennessee 37996

Received December 5, 1997; Revised Manuscript Received March 12, 1998

ABSTRACT: Dynamic light scattering measurements are reported as functions of concentration and temperature for polystyrenes of well defined molecular weight and polydispersity in a good solvent (toluene) and in Θ solvents (cyclohexane, methylcyclohexane, and deuteromethylcyclohexane) in the homogeneous region but under conditions approaching liquid−liquid demixing, including demixing *via* spinodal decomposition. The results are compared with DLS measurements reported in the previous paper for demixing *via* nucleation/growth.

Introduction

Despite longterm and widespread experimental and theoretical interest in the thermodynamics which describe liquid−liquid (LL) phase separation from polymer/solvent and polymer/polymer solutions and similar interest in the mechanism of that process, there seem to have been few light scattering (LS) measurements on solutions very close to precipitation. That is surprising since LS is a technique long used to probe clustering and other size effects in solution. In 1994 Berry elegantly reviewed static light scattering (SLS) and dynamic light scattering (DLS) from moderately concentrated polymer solutions and correlated much of the available experimental information with fundamental theory.[1] He discussed concentration and temperature dependences of LS data in good solvents, and in Θ solvents, but only for temperatures at T_Θ or to its homogeneous side. A detailed theoretical description of solutions closer to precipitation, i.e., those lying between T_Θ and the coexistence or cloudpoint surfaces, is complex. It is not yet developed in sufficient detail to properly interpret the few experimental data which do exist there. In spite of this difficulty, our interest in the mechanism of LL transitions has prompted us to make LS measurements in the immediate vicinity of the LL transitions, comparing the results, as appropriate, with LS for solutions near T_Θ and above, i.e., ranging into the good solvent region. In this early part of the program we are content with a phenomenological description of the experimental results using scaling theory.

Brown and Nicolai[2] have also reviewed measurements of dynamic light scattering (DLS) from semidilute polymer solutions in good solvents (e.g., toluene, benzene, etc.), and Θ solvents (e.g., cyclohexane) in the homogeneous region far from demixing. Following Wiltzius, Haller, Cannell, and Schaefer[3] they adopted a description which employs a universal master equation based on scaling theory. Solutions in good solvents have been studied most thoroughly. The correlograms can usually be described using a single exponential decay function permitting the definition of a hydrodynamic correlation length, ξ_h, obtained from the cooperative diffusion coefficient of the system, D, using eq 1.

$$\xi_h = k_B T/(6\pi\eta_o D) \tag{1}$$

k_B is Boltzmann's constant, and η_o is the solvent viscosity. D is obtained directly from the single exponential correlogram. The correlograms in Θ solvents are more complex. As concentration increases, the initially simple exponential form changes shape to a more complicated bimodal pattern. The first component, a narrow peak at shorter times, varies linearly with q^2 and is clearly diffusive in nature. The slow peak, which is only important at concentrations above the entanglement concentration, broadens with increasing molecular weight and concentration as its average position shifts toward longer time. The hydrodynamic correlation lengths are determined from the parameters defining the short time decay.[2]

It is commonly assumed that ξ_h is proportional to ξ_s, the static correlation length. ξ_s has been shown to scale logarithmically with concentration as $\log(\xi_s/\text{nm}) = (-0.57 \pm 0.17) - (0.72 \pm 0.01) \log[C/(\text{g mL}^{-1})]$ in good solvents, and $\log(\xi_s/\text{nm}) = (-0.22 \pm 0.08) - (1.0 \pm 0.1) \log[C/(\text{g mL}^{-1})]$ in Θ solvents.[2] These master equations extend over a wide range of molecular weights and include various solvents. For the same good solvents the authors[2] report $\log(\xi_h/\text{nm}) = (-0.28 \pm 0.08) - (0.70 \pm 0.01) \log[C/(\text{g mL}^{-1})]$, concluding that within experimental error ξ_h and ξ_s have the same concentration exponent, one slightly smaller in magnitude than −0.75, which is the value predicted from scaling theory in the good solvent limit. Thus, for good solvents these measurements establish that $\xi_h/\xi_s = 2.0 \pm 0.8$ and that it is concentration independent over the range of the measurements. On the other hand, in the limit of infinite dilution the ratio of correlation lengths ξ_h/ξ_s is known to approach r_h/r_g; r_h is the hydrodynamic radius and r_g the radius of gyration. Fetters, Hadjichristidis, Lindner, and Mays[4] have reviewed careful experiments which establish $r_h/r_g = 0.70 \pm 0.09$ for $10^4 < \text{MW/PS} < 3 \times 10^7$ in a variety of solvents (cyclohexane, benzene, toluene, ethylbenzene, and tetrahydrofuran), and this is in agreement with the value Schmidt and Burchard[5]

* To whom correspondence may be addressed.
[†] Permanent address. Chemistry Department, University of Warsaw, Zwirki i Wigury 101, 02-89 Warsaw, Poland.

S0024-9297(97)01777-4 CCC: $15.00
Published on Web 04/24/1998

report for cyclohexane under Θ conditions, $r_h/r_g = 0.79 \pm 0.04$. Thus, on the basis of work in a variety of solvents and from a number of independent laboratories, it seems clear that the ratio established by concentration scaling in the semidilute region, $\xi_h/\xi_s = 2.0 \pm 0.8$, necessarily drops as concentration falls into the dilute region. Since the scaling relation which describes ξ_s is accurately obeyed to concentrations as low as a few tenths of milligrams per milliliter, i.e. more than an order of magnitude below overlap concentration, $c^* = 3M_w/(4\pi N_{av} r_g^3)$, one concludes that it is the hydrodynamic correlation length, ξ_h, which falls off from the prediction of its scaling relation as concentration falls below c^*. The present paper presents DLS data in cyclohexane above and below the Θ-temperature and in the good solvent toluene to test that hypothesis by examining the validity of the concentration scaling relations at a selection of molecular weights and temperatures. That established, we also report DLS data for cyclohexane, methylcyclohexane, and deuteromethylcyclohexane solutions well below their respective Θ-temperatures and examine the behavior of the correlation functions and the diffusion constants and correlation lengths derived from them as demixing is approached, often at concentrations high enough to ensure spinodal decomposition. The results are usefully compared with DLS correlograms in the nucleation growth region reported in a companion paper.[6]

Although it is generally of interest to compare ξ_s, and ξ_h for identical solutions (at low enough concentration, $\xi_s \rightarrow r_g$, and $\xi_h \rightarrow r_h$), this is not possible in the present case for those solutions with $M_w \leq 4 \times 10^5$. The choice of M_w, dictated by the need in our thermodynamic studies to generate phase transitions and hypercritical points at accessible T, P, and ψ (ψ = segment fraction polymer),[6-8] implies for these solutions that SLS intensities show no q dependence and hence cannot be used as a probe for size effects. In these cases, $r_g < \lambda/20$, which is the usual limit for size determination by SLS.[9] On the other hand, SLS experiments on PS solutions with M_w lower than, e.g., 5×10^5, can give data on virial coefficients and, with proper extrapolation, can be used to define osmotic compressibilities. We plan to report such information for the present series in a separate communication.[10] We have previously discussed the q dependence of DLS intensities for these solutions.[6]

Experimental Section

Materials and Sample Preparation. High purity polystyrene samples of low polydispersity were purchased from Scientific Polymer Products or Pressure Chemical Company and are further specified in Table 1. Reagent grade cyclohexane (CH), methylcyclohexane ($MCHh_{12}$), deuteromethylcyclohexane ($MCHd_{12}$), and toluene (T) were purchased from Aldrich Chemical and used as received except for drying over molecular sieve and filtration as described below. Solutions were prepared gravimetrically and stored in well-capped vials. They were clarified immediately before use by making multiple passes through Millipore polytetrafluoroethylene 0.2 μm filters (Alltech or Whatman) into thoroughly clean dust-free cylindrical Pyrex scattering cells of various dimensions. The LS data improve markedly in quality as cell diameter increases and most of the present data was gathered using cells with $d \sim 12$ mm or greater.

Dynamic Light Scattering. The light scattering measurements were made using a Bookhaven Instruments Corporation package which includes a computer-controlled BI-200SM goniometer, BI-9025AT correlator and signal processor, EMI B2FBK/RMI photomultiplier for photon counting, Spectraphysics model 127 50 mw He−Ne laser, and an associated software package for analysis of static light scattering (SLS) and dynamic light scattering (DLS) data including single and double exponential, CUMULANT, and CONTIN data analysis packages. The instrumentation package provides SLS and DLS data of useful quality for ($15 < \theta < 135$).

Table 1. Properties of Polystyrene Solutions

M_w	1.75×10^4	3×10^4	4×10^5	2×10^6
symbol	PS17.5k	PS30k	PS400k	PS2000k
M_w/M_n[a]	1.06	1.03	1.06	1.30
r_h/nm TOL[g]	2.9	4.0	18	45
CH[g]	2.9	3.8	14	31
MCH[b]	2.5	3.3	13	30
r_g/nm TOL[g]	4.0	5.5	26	67
CH[g]	3.6	4.7	18	41
MCH[b]	3.1	4.1	16	39
c^*/(mg mL) TOL[c]	108	72	9.1	2.6
CH[c]	149	115	28	12
MCH[c]	233	173	36	14
c_{crit}/(mg mL) TOL[d]				
CH[e]			57	30
MCH				
T_{cr}/K TOL[f]	136	141	155	158
CH[f]	277	284	300	304
MCH[f]	296	306	332	339

[a] Manufacturer's specification. [b] From low concentration limit present experiments on PS17.5k and followed by MW scaling using the expression for CH given in ref 4. [c] $c^* = 3M_w/(4\pi N_{av} r_g^3)$. [d] No phase transition in this solvent. [e] Calculated from the scaling relation,[15] $\ln(\phi_c) = 2.04 - 0.385 \ln(M_w)$, and density data; ϕ_c is the volume fraction PS at the critical point. [f] From ref 8. [g] From ref 4.

For scattering measurements the sample cells were centered in a thermostated bath filled with toluene for refractive index matching at ±~0.01 K. The toluene bath is slaved to an external master circulating thermostat (model 704 Hart Scientific, ±~0.001 K). An independently pumped circulation/filter system removes dust but is turned off during LS measurements. For temperature quenches the master thermostat is manually adjusted to provide the desired heating or cooling rate. The precision of thermostating at the scattering cell has deteriorated about an order of magnitude from the master bath but, nonetheless, remains adequate for our purposes. Sample to sample reproducibility of phase transition temperatures was ~±0.1 K, but run to run reproducibility for given samples was better, (~±0.02−0.05 K).

Viscosity and Density. Viscosities and densities were obtained from standard sources.[11,12]

Results and Discussion

This work compares DLS correlation lengths, ξ_h, and/or DLS derived diffusion coefficients, D, for polystyrene (PS) of various molecular weights in toluene (T), cyclohexane (CH), and protio- and deuteromethylcyclohexane ($MCHh_{12}$ and $MCHd_{12}$). The measurements were made at a 90° scattering angle, except in each case we checked scattering at several lower angles to ensure that the reported ξ_h values correspond to diffusive motion.[6]

Toluene Solutions. The concentration dependence of ξ_h was determined for PS solutions, $M_w = 3 \times 10^4$, 4×10^5, and 2×10^6 amu, all at 25.5 °C (298.65 K), comfortably in the good solvent region for toluene. Parameters of interest, including reduction parameters, are reported in Table 1. The low concentration limit for the measurements was dictated by scattering intensity. The high concentration limit was set by the quality of the derived correlation radii, which deteriorates with developing bimodal character at high concentration (vide supra). Even so, we observed bimodality only at the very highest concentrations and the present data are not influenced by this effect.

Table 2. Empirical Representations of DLS Correlation Radii

I. PS in Toluene at 25.5 °C: $\log(\xi_h/\text{nm}) = b(0) + b(1)[\log(c)] + b(2)[\log(c)]^2$

sample	range[a] (mg/mL)	no. of points	$b(0)$	$b(1)$	$b(2)$	r^2
PS2000k	0.3−51	11	1.49445	−0.20555	−0.17987	0.995
PS400k	0.9−197	19	1.16779	−0.06891	−0.09636	0.992
PS30k	4.4−270	19	0.43845	0.14947	−0.08699	0.931

II. PS2000k in Cyclohexane: $\log(\xi_h/\text{nm}) = b(0) + b(1)[\log(c)] + b(2)[\log(c)]^2$

temp (°C)	range (mg/mL)	no. of points	$b(0)$	$b(1)$	$b(2)$	r^2
36.2	2−21	7	1.46746	0.17801	0.10597	0.989
48.2	2−21	7	1.49378	0.23784	−0.26631	0.998

III. PS400k in Cyclohexane: $\log(\xi_h/\text{nm}) = c(0) + c(1)(t/°\text{C}) + c(2)(t/°\text{C})^2 + c(3)(t/°\text{C})^3 + ...$

sample (mg/mL)	range[a] (°C)	no. of points	$c(0)$ $c(4)$	$c(1)$ $c(5)$	$c(2)$	$c(3)$	r^2
0.15	23−41	5	1.0146	3.528E−3			0.968
0.41	23−41	5	1.0381	3.065E−3			0.964
0.51	23−41	5	1.0544	2.682E−3			0.988
0.61	23−41	5	1.0614	2.527E−3			0.983
0.81	23−41	5	1.0790	2.106E−3			0.960
1.1	23−41	5	1.1035	1.516E−3			0.986
6.4	25−43	13	3.3891	−0.18358	5.226E−3	−4.977E−5	0.967
9.4	25−43	11	3.7316	−0.17768	4.351E−3	−3.644E−5	0.998
12.4	30−43	4	1.5541	−6.441E−3			0.966
28.9	26−43	10	616.28	−88.3921	5.0676	−0.1446	
			2.055E−3	−1.162E−5			0.998
80	26−40	22	46.480	−3.7634	0.1056	−9.941E−4	0.991
103.7	27−39	14	51.675	−4.2119	0.1188	−1.1244E−3	0.996

IV. PS17.5k in Methylcyclohexane: $\log(\xi_h/\text{nm}) = c(0) + c(1)(t/°\text{C}) + c(2)(t/°\text{C})^2 + c(3)(t/°\text{C})^3 + ...$

sample (mg/mL)	range[a] (°C)	no. of points	$c(0)$ $c(4)$	$c(1)$ $c(5)$	$c(2)$	$c(3)$	r^2
1.15	8−20	8	0.6126	4.733E−3			0.744
2.9	8−33	15	0.8555	−0.01447	4.163E−4		0.769
5.8	12−33	15	0.8474	−6.584E−3	1.130E−4	1.615E−6	0.732
11.6	13−33	14	0.9907	−0.01502	3.104E−4	6.177E−7	0.950
23.2	19−33	11	1.5903	−0.07109	2.392E−3	−2.632E−5	0.947
51.5	20−33	10	2.2026	−0.08422	1.964E−3	−1.408E−5	0.995
72.8	23−36	16	7.0084	−0.54697	0.01661	−1.702E−4	0.992
92.8	22−33	9	3.2239	−0.11458	1.650E−3		0.994
101	23−36	11	13.6856	−1.12814	0.03395	−3.4421E−4	0.997
124	23−40	17	66.69215	−7.86801	0.35491	−7.105E−3	
			5.311E−5				0.994
155	24−41	18	102.81059	−12.23868	0.55342	−0.01109	
			8.2975E−5				0.990
170	23−41	12	232.36545	−29.7904	1.4415	−0.03092	
			2.478E−4				0.992
200	24−41	16	161.71719	−19.3785	0.87580	−0.01751	
			1.305E−4				0.979
220	23−41	32	39.6926	−3.9860	0.15755	−2.770E−3	
			1.816E−5				0.988
248	23−42	19	129.23099	−15.3569	0.68908	−0.01367	
			1.010E−4				0.992
315	24−38	12	21.42618	−1.78081	0.054059	−5.573E−4	0.999
359	27−47	8	13.62425	−0.89908	0.022111	−1.837E−4	0.987

V. PS30k (0.109 = $(n(\text{monomer})/(n(\text{monomer}) + n(\text{solvent}))$) in MCHh/MCHd Mixtures:
$\log(\xi_h/\text{nm}) = c(0) + c(1)(t/°\text{C}) + c(2)(t/°\text{C})^2 + c(3)(t/°\text{C})^3 + ...$

sample y_D	range[a] (°C)	no. of points	$c(0)$ $c(4)$	$c(1)$ $c(5)$	$c(2)$	$c(3)$	r^2
MCHd = 0.00	33−45	25	800.12866	−79.7578	2.98718	−0.04971	
			3.099E−4				0.994
MCHd = 0.35	34−50	19	238.15631	−21.65396	0.74360	−0.011354	
			6.498E−5				0.995
MCHd = 0.49	34−51	17	330.12682	−29.86392	1.01674	−0.015364	
			8.687E−5				0.992
MCHd = 0.61	35−52	20	208.52922	−17.9812	0.58575	−8.480E−3	
			4.599E−5				0.997
MCHd = 0.77	36−48	24	700.07325	−64.6372	2.24226	−0.03455	
			1.994E−4				0.997
MCHd = 1.00	34−50	19	34.49771	−2.02597	0.041610	−2.8676E−4	0.999

[a] The term "range" indicates the extent of the empirical polynomial fit. In some cases one or two data points furthest from the phase transition (i.e., at the highest temperature or lowest concentration depending on the type of fit) were dropped in order to improve the quality of fit to the remaining data. These points, however, are included in the figures reported in this paper. The empirical representations given in this table are strictly for interpolation and cannot be used for purposes of extrapolation.

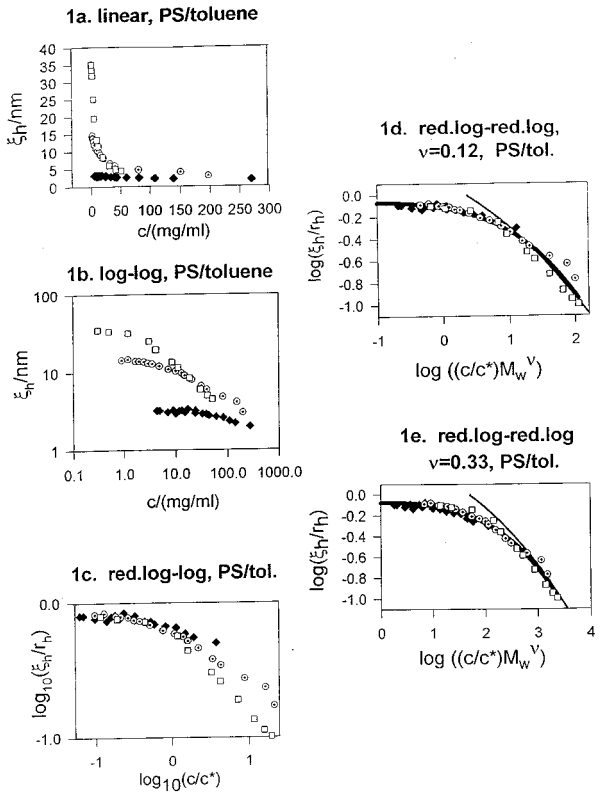

Figure 1. Concentration and MW dependence of DLS hydrodynamic correlation radii for polystyrene/toluene solutions, $M_w = 3 \times 10^4$, 4×10^5, and 2×10^6 amu at 298.65 K. In parts a−e, open squares = PS2000k, open circles = PS-400k, and shaded diamonds = PS-30k. (a) The linear−linear representation, ξ_h/(nm) vs c/(mg mL^{-1}). (b) Log−log representation. (c) Logarithmic reduced correlation radius, ξ_h/r_h vs logarithmic reduced concentration, ln(c/c^*), $c^* = 3M_w/(4\pi N_{av} r_g^3)$. (d) Logarithmic reduced correlation radius vs logarithmic reduced and M_w scaled concentration, $\nu = 0.12$. The light solid line is calculated from limiting expressions given by Brown and Nicolai[2] and Fetters et al.[4] The heavy solid line is the least-squares fit to eq 2 reported in Table 3. (e) Logarithmic reduced correlation length vs logarithmic reduced and M_w scaled concentration. $\nu = 0.33$. The light solid line is calculated from limiting expressions given by Brown and Nicolai[2] and Fetters et al.[4] The heavy solid line is a least-squares fit to eq 2 reported in Table 3.

DLS data showing the concentration dependence of hydrodynamic correlation radii of PS solutions at three M_w's are reported in Table 2 and shown in Figure 1. Figure 1a is a linear representation in (ξ_h,c) space, and Figure 1b shows the same data in a double logarithmic plot. These representations demonstrate that $\partial(\log \xi_h)/\partial(\log c)$, uniformly negative in this good solvent system, drops off as concentration increases. Figure 1c represents the data logarithmically in (c/c^*, ξ_h/r_h) space. The reduction parameters are the hydodynamic radii, r_h ($r_h = \lim_{\{c\to 0\}} \xi_h$), and the overlap concentration, $c^* = 3M_w/(4\pi N_{av} r_g^3)$. For $c/c^* > 1$ the curves are offset from each other because M_w scaling is not yet included. Figure 1d shows the data reduced yet again; $\log[(c/c^*)M_w^{\nu}]$ defines the abcissa. The exponent $\nu = 0.12$ is that chosen by Brown and Nicolai[2] (BN) who reviewed literature data and demonstrated nearly linear double logarithmic scaling in the high concentration, high molecular weight limit, $\log(\xi_h/r_h)$ vs $\log(k_D c)$. Here k_D is the first expansion coefficient for $D_c = D_0(1 + k_D c + \ldots)$. D_c is the DLS diffusion constant for a series of high M_w PS's in good solvents with $c > c^*$. The M_w dependence enters through k_D via the correlation in Figure 6 of ref 2. Our fit to that data yields $\log(k_D) = (0.70 \pm 0.07) \log(M_w) - (1.92 \pm 0.46)$. Transformation to the present representation gives $\nu = 0.12 \pm 0.08$ and demonstrates that the weak M_w dependence of the correlation is not well-defined. In Figure 1d the heavy solid line represents an empirical fourth-order least-squares correlation forced to asymptotically approach $\xi_h/r_h = 1$ from below as $c \to 0$. The parameters are reported in Table 3. Simpler representations do not accurately represent the curvature.

$$\log[\xi_h/r_h] = \sum a_i[\log((c/c^*)M_w^{\nu})] \quad (0 < i < i_{max}) \qquad (2)$$

The lighter line in Figure 1d represents the BN high M_w, $c > c^*$ correlation expressed in the present coordinates (see Table 3). It is clear that the present data nicely approach the BN limit at high $(c/c^*)M_w^{\nu}$. Figure 1e shows a mildly improved correlation, this time using the empirically chosen $\nu = 0.33$. The data are more tightly grouped about the fourth-order correlation line than in Figure 1d, and the high M_w, $c > c^*$ approach to the limiting slope is a little better. We think that even though $\nu = 0.33$ lies outside the bounds of the rms fit to the BN correlation, $\nu_{BN} = 0.12 \pm 0.07$, it is to be preferred because it more accurately represents scaling in the high-c region. The BN correlation hinges upon the definition of the M_w dependence of the zero concentration limit of $\partial D_c/\partial c \sim \partial(1/\xi_h)/\partial c$. It must deteriorate as concentration increases. The present more empirical approach is not so limited; this rationalizes the observation that the empirically chosen $\nu \sim 0.33$ is different from that in the BN limit, $\nu \sim 0.12$. Parts d and e of Figure 1 demonstrate reasonable convergence of DLS data to master curves defining the hydrodynamic correlation lengths over broad ranges of concentration and M_w.

Cyclohexane and Methylcyclohexane Solutions. DLS studies in PS/CH and PS/MCH solutions were undertaken because the literature shows in good solvents, and in Θ solvents for T well above T_Θ,[2] ξ_h decreases with concentration ($d(\log(\xi_h))/d(\log(c)) < 0$), but our preliminary studies in MCH and CH not too far from the LL phase transition gave $d(\log(\xi_h))/d(\log(c)) > 0$ even for PS solutions of modest MW at low concentration. Most literature data refer to solutions of higher M_w well above T_Θ.

We first discuss results for PS2000k/CH, Figure 2a. These data extend from 2 to 21 mg/mL. At this high MW, DLS measurements are difficult because the samples show considerable opalescence accompanied by large intensity fluctuations. The fluctuations increase markedly with concentration and are accentuated at low scattering angle. The data presented in Figure 2 were developed using cumulant analysis (except at the single highest concentration where CONTIN was employed). At low concentrations, the agreement between CUMULANT and CONTIN is quantitative. The DLS pattern is bimodal only at the highest concentration. The smaller component is diffusive and is the one plotted in the figure. The larger nondiffusive mode is found at ~2000 nm or more and is typical of the features described by Brown[2] as "transient network coupling modes" or ascribed by Sun and Wang[13] to coupling between concentration and density fluctuations. The raw data from Figure 2a, scaled analogously to the toluene data shown in Figure 1e, are replotted in Figure 2b where they are compared with the good solvent (T)

Table 3. Least-Squares Parameters of Fit to Eq 2

$$\log[\xi_h/r_h] = \sum a_i[\log((c/c^*)M_w^{\nu})]^i$$

ν	a_0	a_1	a_2	a_3	a_4	r^2
			PS/Toluene: All Data Points in Figure 1			
0.12	−0.115832	−0.104690	−0.082692	−0.025626	−2.477169E−3	0.962
			PS/Good Solvent Correlation of Ref 1 Expressed Using Present Coordinates			
0.12	0.117658	−0.293257	−0.114286			
			PS/Toluene: All Data Points in Figure 1			
0.33	−0.075792	−2.526300E−3	−0.016112	−0.012558	−1.795127E−3	0.982
			PS/Good Solvent Correlation of Ref 1 Expressed Using Present Coordinates			
0.33	0.305344	0.014171	−0.114286			

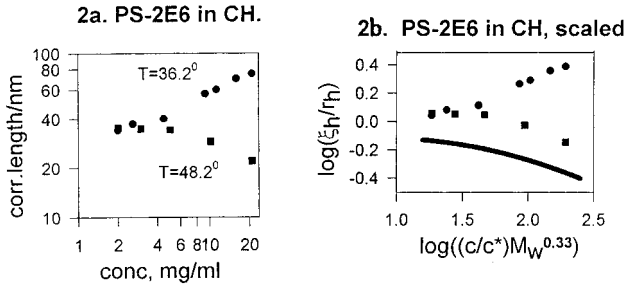

Figure 2. Hydrodynamic correlation radii of polystyrene/cyclohexane solutions. (a) Log−log representation, log(ξ_h/(nm)) vs log(c/(mg mL^{-1})), for PS2000k/CH solutions at 36.2 (upper curve) and 48.2 °C (lower curve). (b) Log−log scaled representation, ln(ξ_h/r_h) vs ln($(c/c^*)M_w^{0.33}$), for PS2000k/CH 48.2 °C (solid squares) and 36.2 °C (solid circles). The heavy solid line shows a portion of the correlation for PS-T solutions from Figure 1e and Table 3; $\nu = 0.33$.

smoothing relation from Table 3 and Figure 1. The concentration range of the present measurements is too high to permit reasonable extrapolation to infinite dilution and thus precludes an independent determination of limiting diffusion coefficients and hydrodynamic radii.

The most prominent feature of the PS2000k/CH data is the change in slope, $\partial\log(\xi_h)/\partial\log(c)$, which goes from positive to negative as temperature rises from 36 °C (just above T_Θ; see Table 2) to 48 °C (comfortably above T_Θ). Apparently there exists a temperature (∼42 °C) where $\partial(\log(\xi_h))/\partial(\log(c)) \sim 0$ over a considerable range of concentration. As pointed out earlier, $d(\log(\xi_h))/d(\log(c)) \sim -0.7$ for good solvents in the high c, high M_w limit, and it seems the PS-2E6/CH data will approach that correlation at sufficiently high concentration for ($t >$ ∼48). The increase in slope as T drops toward T_Θ and into the poor solvent region is of interest. It is connected with the "slowing down" of DLS diffusion processes, ($D_c \sim \xi_h^{-1}$; see eq 1), observed on the approach to the coexistence curve and critical point,[14] vide infra.

We have also gathered extensive (T, ξ_h, c) datanets for PS400k/CH [(23 < t/°C < 44) and (0.15 < c/(mg mL^{-1}) < 108)] and PS17.5k/MCH [(8 < t/°C < 48) and (1.15 < c/(mg mL^{-1}) < 359)] solutions in order to study the approach to LL demixing along the upper consolute branch. Methylcyclohexane (MCH) is not as good a solvent as CH. Its use permitted us to adjust the LL transition temperature to a convenient value, i.e., at lower MW, in order to enjoy the advantages of lower viscosity and lower background opalescence as the LL transition is neared. Heretofore there have existed a paucity of DLS data at temperatures and concentrations close to LL demixing,[2] and the quantitative and qualitative features of the correlograms in this region are of interest.

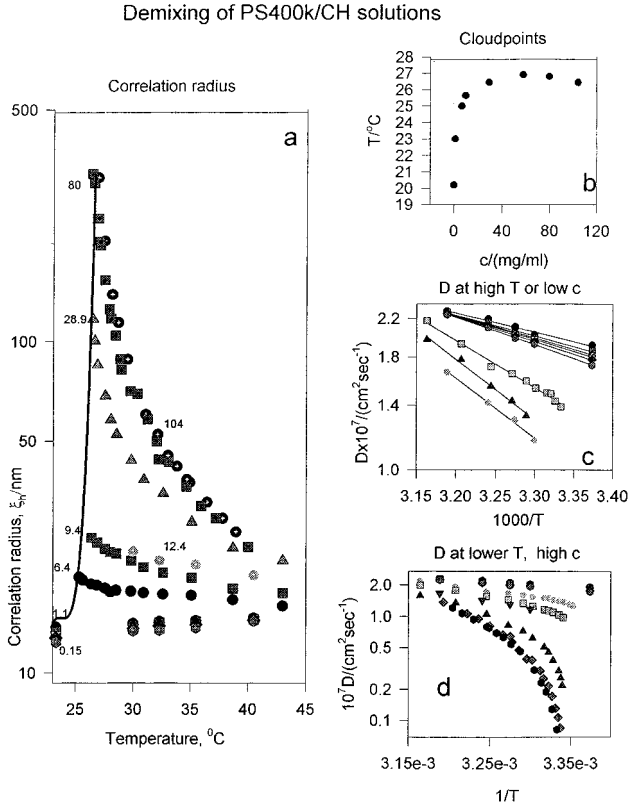

Figure 3. DLS-derived correlation radii, diffusion constants and cloud points for PS400k/CH solutions. (a) Logarithmic plot of correlation radius vs temperature at various concentrations, reading down at the phase transition line, 104, 80, 28.9, 12.8, 9.4, and 6.4 mg/mL, and then very closely spaced at 1.1, 0.81, 0.61, 0.51, 0.41, and 0.15 mg/mL. (b) Visual cloud points for the solutions in part a. An empirical line for use in interpolation is given by the least-squares equation {[t(CP)/°C] = 22.89 + 2.987 [log(c/(mg/mL))] + 0.128 [log(c/(mg/mL))]^2 − 0.339 [log(c/(mg/mL))]^3, r^2 = 0.996. (c) DLS-derived diffusion coefficients for data from part a in the region where linear plots in the (log(D), 1/T) plane are well behaved, (i.e., at lower concentrations and/or higher temperature ranges): reading up at 12.8, 9.4, 6.4, 1.1, 0.81, 0.61, 0.51, 0.41, and 0.15 mg/mL. (d) DLS-derived diffusion coefficients, for all data in part a: reading up at 104, 80, 28.9, 12.8, 9.4, and 6.4 mg/mL and then closely spaced at 1.1, 0.81, 0.61, 0.51, 0.41, and 0.15 mg/mL.

DLS data for PS400k/CH and PS17.5k/MCH solutions are reported in Table 2 and shown in the (ξ_h, T), (D, 1/T), and (D, c) projections in Figures 3 and 4. The DLS patterns defined by these data sets are in excellent qualitative agreement with one another and are in complete accord with the qualitative discussion given in the introduction of the companion paper and sketched there in Figure 1.[6] Figures 3a and 4a (for PS400k/CH and PS17.5k/MCH, respectively), for T significantly

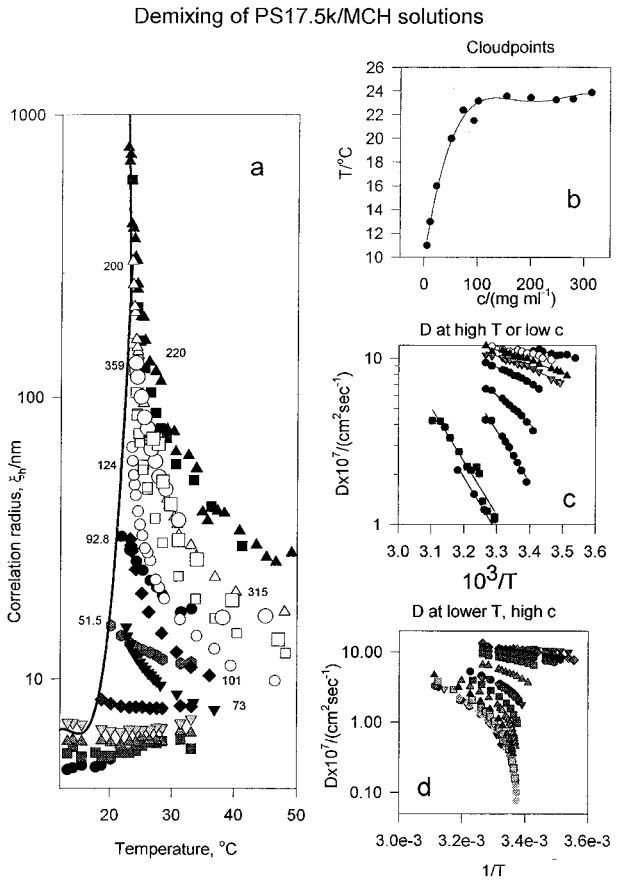

Figure 4. DLS-derived correlation radii, diffusion constants and cloud points for PS17.5k/MCH solutions. (a) Logarithmic plot of correlation raduis vs temperature at various concentrations: reading up at phase transition line, 1.15, 2.9, 5.8, 11.6, 23.2, 51.5 (shaded octagons), 72.8 (inverted triangles), 92.8 (solid circles), 124 (open circles), 155 (open squares), 200 (open triangles), 315 (large open circles), 359 (large open squares), 170 (shaded squares), and 220 mg/mL (solid triangles). Numerical labels locate some of the lines. To avoid clutter not all data reported in Table 2 has been plotted. (b) Visual cloud points for the solutions in part a. An empirical line for use in interpolation is given by the least-squares equation $\{[t(\mathrm{CP})/°\mathrm{C}] = 9.81 + 0.2953\ [\log(c/(\mathrm{mg/mL}))] - 2.291 \times 10^{-3}\ [\log(c/(\mathrm{mg/mL}))]^2 + 7.466 \times 10^{-6}\ [\log(c/(\mathrm{mg/mL}))]^3 - 8.642 \times 10^{-9}\ [\log(c/(\mathrm{mg/mL}))]^4$; $r^2 = 0.987\}$. (c) DLS-derived diffusion coefficients for data from part a in the region where linear plots in the (log(D), 1/T) plane are well behaved, (i.e., at lower concentrations and/or higher temperature ranges): reading down 1.15, 2.9, 5.8, 11.6, 23.2, 92.8, 170, and 220 mg/mL. (d) DLS-derived diffusion coefficients, with all data in Table 2, including 1.15, 2.9, 5.8, 11.6, 23.2, 51.5, 73, 92.8, 101, 124, 170, 200, 220, 248, 284, 315, and 359 mg/mL. The curves are in inverse order to that described in the caption to part a.

larger than T_Θ, or ψ small enough (e.g., $\psi/\psi_{cr} \sim 1/10$ or less), or both, show that the DLS correlation length approaches its hydrodynamic limit in a smooth and well-behaved fashion. At low enough c the approach is from below; at higher concentration, it is from above (i.e., at low c, $(\partial(\log \xi_h)/\partial T) > 0$ while at high c, $(\partial(\log \xi_h)/\partial T) > 0$). Figures 3b and 4b report visual cloud points (CPs) in the (T, c) plane. In each case there is an abrupt rise to a broad plateau. Neither CP diagram looks at all like the standard textbook example. CP loci from Figures 3b and 4b have been included in Figures 3a and (4a). To do so, we employed the equations in Table 2 to empirically estimate correlation radii and the CP for each solution and have shown the results as the heavy solid lines.

Table 4. Empirical Representations of DLS-Defined Diffusion Coefficients for Concentrations and Temperatures Where $\log(10^7 D/(\mathrm{cm^2\ s^{-1}})) = D(0) + D(1)/T$ or Fits the Data to Useful Approximation[a]

c/(mg/mL)	$D(0)$	$D(1)$	r^2	no. of points
Solution: PS400k/CH				
0.15	1.740	−432.9	0.982	5
0.41	1.871	−475.5	0.991	5
0.51	1.979	−509.6	0.999	5
0.61	2.048	−531.6	0.999	5
0.81	2.142	−561.4	0.998	5
1.1	2.330	−620.2	0.999	5
6.4	3.714	−1069	0.989	10
9.4	4.639	−1371	0.992	5
12.8	4.566	−1362.	0.993	4
Solution: PS17.5k/MCH				
1.15	2.239	−348.7	0.836	8
2.9	2.732	−502.8	0.809	11
5.8	3.296	−680.5	0.977	15
11.6	3.551	−769.1	0.965	14
23.2	4.058	−943.1	0.988	11
51.5	6.480	−1729	0.975	10
92.8	10.668	−3062	0.972	9
170	10.925	−3324	0.971	8
220	10.708	−3227	0.938	5

[a] Note for $10^7 D/(\mathrm{cm^2\ s^{-1}}) = \exp(A)\exp(-E_{a,D}/RT)$ that $D(0) = A\log(e)$ and $D(1) = (-E_{a,D}/R)\log(e)$.

At low enough concentration, and/or far enough from the LL demixing locus, the DLS diffusion constants plot as good straight lines in the (log(D), 1/T) plane, yielding sets of well-behaved activation energies for diffusion, (Figures 3c and 4c).

$$\ln(D) = A - (E_{a,D}/R)/T \quad (0.15 < c/(\mathrm{mg/mL}) < 12.8) \tag{4}$$

Values of [A log(e)] and [($E_{a,D}/R$) log(e)] are reported in Table 4. At higher concentrations, (c > 12 mg/mL) curvature in (log(D), 1/T) increases to the point where this kind of analysis is no longer useful (see Figures 3d and 4d). At the lower concentrations, however, smooth trends in e^A and $E_{a,D}$ with concentration are observed. These are reported in parts a and b of Figure 5. Equations of the least-squares correlating lines are given in the captions.

In Figure 6 we continue to explore DLS effects near the low concentration limits of the study. Figure 6a shows the concentration dependence of D at selected temperatures for $c/c^* \ll 1$, and Figure 6b reports the temperature dependence of the zero concentration intercepts, D_o, over the temperature range of the measurements. The parameters of the least-squares correlation lines are reported in the captions. Hydrodynamic radii, $r_h = \xi_h{}^o$, are straightforwardly recovered using eq 1.

The practical high concentration limit for DLS measurements in these solutions lies at or slightly above the critical concentration, c_{cr}, estimated from Figures 3 and 4 to lie in the range ($80 < c_{cr}/(\mathrm{mg/mL}) < 104$) for PS400k/CH, and ($200 < c_{cr}/(\mathrm{mg/mL}) < 250$) PS17.5k/CH, as is common assuming criticality lies just to the high concentration side of the maximum in CP. An alternate estimate for PS400k/CH using a scaling relation recommended by Melnichnko[11] yields $\psi_{cr} \sim 57$ g/mL (~6.8 wt %). That latter value is simply too low according to the present cloud point data, Figure 3b. Both CP diagrams (Figures 3b and 4b) show marked asymmetry and extended flat portions in the region of the maxima. Consequently it is difficult to define c_{cr} with precision.

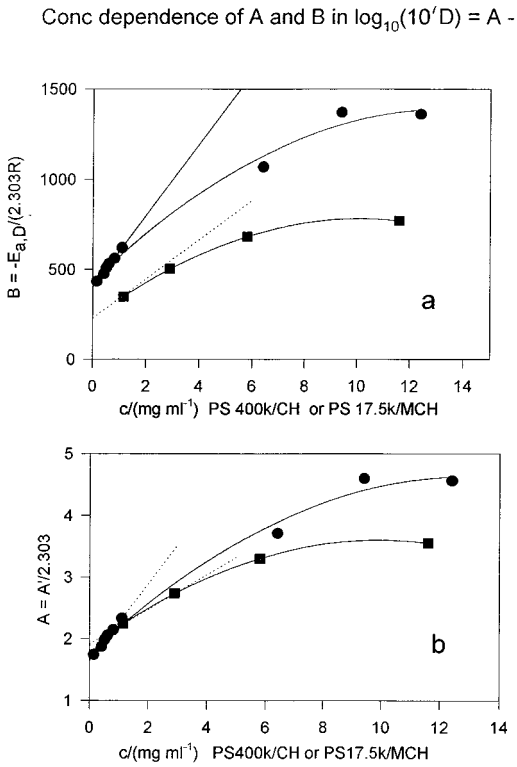

Figure 5. Concentration dependences of A and B for data presented in Table 4 and Figures 3c and 4c, $\log(10^7 D/(\mathrm{cm}^2\ \mathrm{s}^{-1})) = A + B/T$. Since $\ln(10^7 D/(\mathrm{cm}^2\ \mathrm{s}^{-1})) = A' - E_{a,D}/(RT)$, $A = A'/2.303$ and $B = -E_{a,D}/2.303R$. (a) Fits of B: solid circles = PS400k/CH, where the limiting line is described by $B = 403.5 + 198.1$ (c/(mg/mL)) and the curved line by $B = 436 + 143$ (c/(mg/mL)) $- 5.34$ (c/(mg/mL))^2; solid squares = PS17.5k/CH, where the correlation line is $A = 230 + 109$ (c/(mg/mL)) $- 5.41$ (c/(mg/mL))^2 and the limiting slope obtained from this equation is underestimated. (b) Fits of A: solid circles = PS400k/CH, where the limiting dotted line is described by $A = 1.64 + 0.625$ (c/(mg/mL)) and the curved line by $A = 1.75 + 0.44$ (c/(mg/mL)) $- 0.017$ (c/(mg/mL))^2; solid squares = PS17.5k/CH, where the correlation line is $A = 1.86 + 0.35$ (c/(mg/mL)) $- 0.018$ (c/(mg/mL))^2 and the limiting slope calculated from this equation is underestimated.

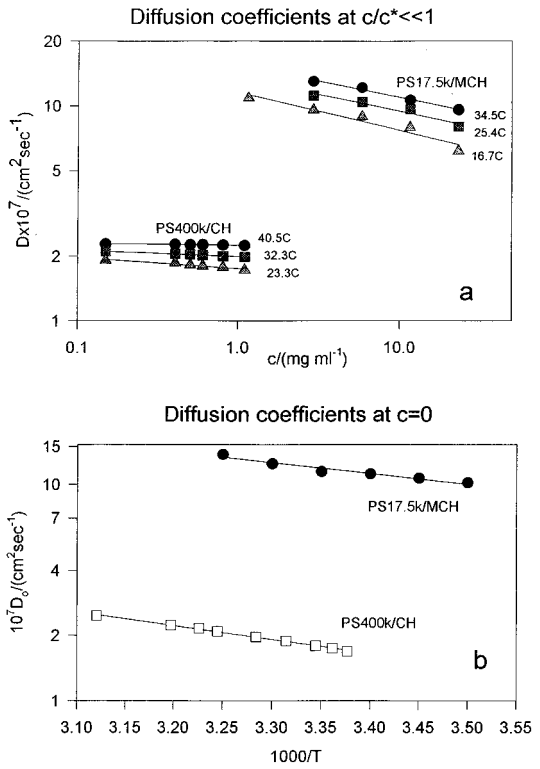

Figure 6. Behavior of the DLS diffusion coefficients at low concentration: (a) concentration dependence at (c/c^*) $\ll 1$ at selected temperatures for PS17.5k/MCH and PS400k/CH solutions; (b) temperature dependence of limiting ($c = 0$) DLS diffusion coefficients for PS17.5k/MCH and PS400k/CH solutions. The correlating equations are as follows: PS17.5k/MCH, $\log(10^7 D_o/(\mathrm{cm}^2\ \mathrm{s}^{-1})) = 2.74 - 497/(T/\mathrm{K})$; PS400k/CH, $\log(10^7 D_o/(\mathrm{cm}^2\ \mathrm{s}^{-1})) = 2.40 - 641/(T/\mathrm{K})$.

The logarithmic discontinuity in correlation radius, ξ_h, expected at c_{cr} (Figures 3a and 4a) is matched by an exponential fall-off in D as the critical conditions are approached (Figures 3d and 4d). A critical falling-off has been discussed at length for small molecule solutions by Ikier, Klein, and Woermann.[14] It is already becoming apparent in PS400k/CH as concentration increases above 28.9 (Figure 3d) or 101 mg/mL PS17.5k/MCH (Figure 4d), but perhaps is better illustrated using alternate plots in the (D, T) plane. In Figure 7a we plot D vs ($T - T_{cloud}$) in the vicinity of the minimum in D (i.e., not too far from the critical concentration). The diffusion constants fall by more than 1.5 orders of magnitude as the demixing curve in the vicinity of the critical point is approached. Data at higher or lower concentrations show appreciable curvature in these projections. Figure 7b presents an alternate view of the same effect. Here we plot ξ_h vs log(c). The anticipated sharp rise at c_{cr} is clearly indicated for both sets of solutions. It is unfortunate that for these inconveniently viscous solutions we were unable to make measurements at appreciably higher concentrations in order to more thoroughly investigate the approach to criticality and critical falling-off from above.

Reduced Representation: PS/TOL, PS/CH, and PS/MCH Data. Figure 8a collects the entire data net, that for all solutions, onto a single plot. The representation is the same as that used in Figure 1c. In the poorer solvents ξ_h/r_h begins to rise from its low concentration/high temperature limit of 1 around $c/c^* = 0.2$, and as concentration increases, it departs further and further from the reference value, $\xi_h/r_h = 1$. What at first glance is a rather broad envelope enclosing badly scattered data, under closer examination reduces to a regular temperature-dependent progression. As expected, the deviation increases rapidly as the temperature drops toward T_{cr} and/or the concentration increases above $c/c^* \sim 2$ or more. This behavior is made clear in Figure 8b which shows smoothed values of ξ_h/r_h at reduced temperatures, T/T_{cr}, between 1.00 and 1.04. Although plots like the ones in parts a and b of Figure 8 clearly establish the qualitative features of the concentration and temperature dependences of reduced DLS correlation lengths in these various solvents, the scatter which remains is too large to permit the report of a single smoothing function to describe the data, which, we feel, are better and more appropriately represented graphically.

The H/D Solvent Isotope Effect for Demixing: PS30k/MCHh$_{12}$/MCHd$_{12}$ Solutions. Solvent isotope effects on demixing are of special interest because deuterated solvents are widely employed in neutron scattering studies of polymer solutions.[16] This fact, together with a longstanding interest of this laboratory on isotope effects in solution thermodynamics, prompted us to make a set of DLS measurements for demixing from a mixed H/D solvent system at near critical conditions. We elected to study PS30k/MCH since

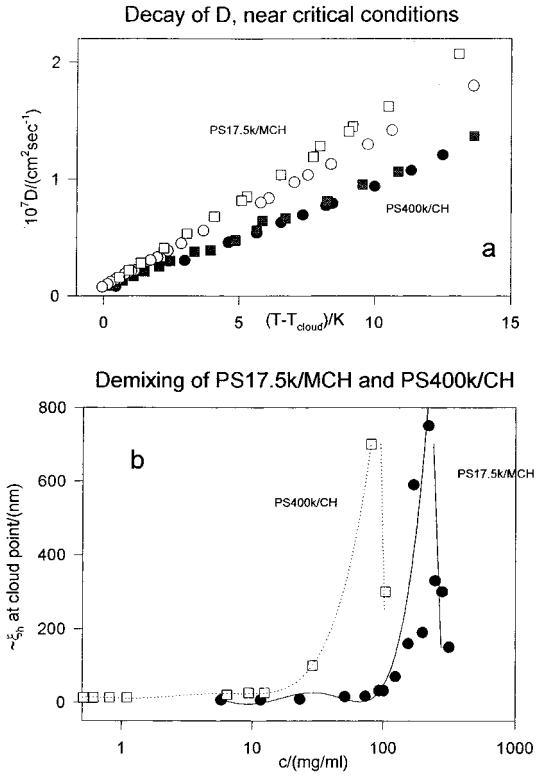

Figure 7. Diffusion constants and correlation radii near c_{cr}. (a) Temperature dependence of D for several solutions not too far from c_{cr}: solid points, PS400k/CH (squares = 104 mg/mL; circles = 80 mg/mL); open points, PS17.5k/MCH (squares = 248 mg/mL; circles = 200 mg/mL). The diffusion constant vanishes as T_{cp} is approached for these near-critical solutions. (b) Concentration dependence of ξ_h for several solutions: open squares, PS400k/CH; solid circles, PS17.5k/MCH. In each case the infinity in ξ_h (zero in $D \sim \xi_h^{-1}$) at the critical concentration is clearly indicated. The low concentration ripple in the PS17.5k/MCH data is an artifact introduced by the plotting program used to draw the solid line.

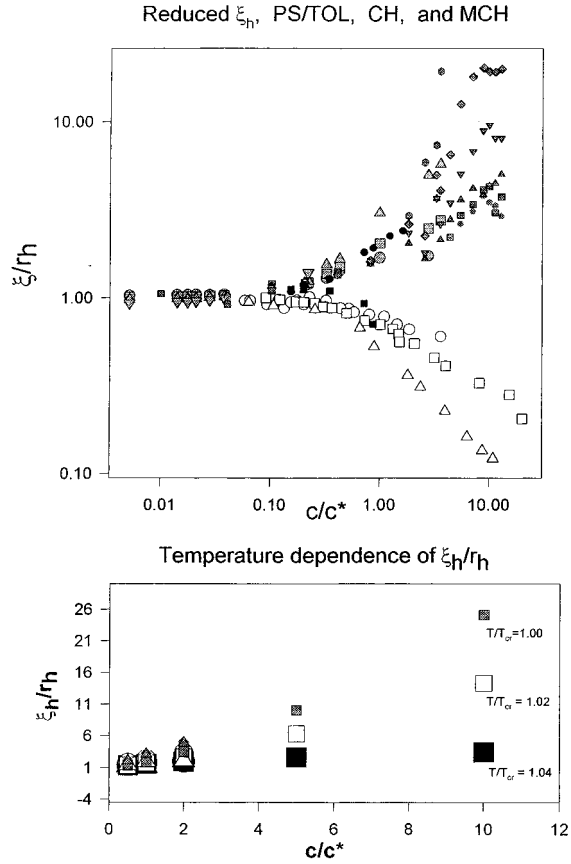

Figure 8. (a) Reduced DLS correlation radii as a function of reduced concentration, double logarithmic representation for all solutions. Open data points PS/TOL are the same as in Figure 1c. Solid squares = PS2000k/CH at 48.2 °C; solid circles = PS2000k/CH at 38.2 °C. Large shaded points refer to PS400k/CH solutions at temperatures falling from $T/T_{cr} = 1$ at the top of the upper band to $T/T_{cr} = 1.04$ at the bottom. Similarly the small shaded points refer to PS17.5k/MCH solutions at temperatures falling from $T/T_{cr} = 1$ at the top of the upper band to $T/T_{cr} = 1.04$ at the bottom. This point is further developed in part b. (b) The concentration dependence of reduced correlation radii for PS2000k/CH, PS400k/CH, and PS17.5k/MCH solutions smoothed and represented at three reduced temperatures: $T/T_c = 1.04$ solid; $T/T_c = 1.02$ open; $T/T_c = 1.00$ shaded. PS2000k/CH = triangles, PS400k/CH = circles, and PS17.5k/MCH = squares. The use of variously sized symbols permits superposed points to be shown.

critical precipitation from this solution is in a convenient part of the phase diagram.

Figure 9a plots DLS correlation radius vs temperature for solutions (0.109 segment fraction) of near critical concentration and ($0 < [y_D = D/(H + D)] < 1$). The CP diagram is flat in the vicinity of the critical point (cf. Figures 3a and 4a) and in each case is not expected to vary more than a few tenths Kelvin over the range of reduced concentrations, $c_r = |c - c_{cr}|/c_{cr}$, exhibited by this series of solutions. Accordingly, corrections for small deviations from the critical concentration are unnecessary at the present level of precision. The DLS correlograms are monomodal and well behaved. Least-squares representations of the (ξ_h, T) plane are reported in Table 2. The expected near-critical divergence in correlation length as the demixing line is approached is evident in Figure 9a. The solvent isotope effect on the critical temperature is $[(T_{cr}(MCHd_{12}) - T_{cr}(MCHh_{12})] = (T_{cr,d} - T_{cr,h}) = 3.7 \pm 0.2$ K. Visual cloudpoint temperatures and transition temperatures determined from the empirical determined zeros in fits to the (D, T) data are reported in Table 5 and are shown in Figure 9b. The agreement is satisfactory. The figure indicates the deviation of the fit to (T_{cp}, y_D) from linearity is small, certainly not more than two or three standard deviations. It establishes the $MCHh_{12}/MCHd_{12}$ as nearly ideal in this region of the phase diagram according to the formalism introduced by Singh and Van Hook[17] and further discussed by Luszczyk and Van Hook.[7] This is not surprising, as under present conditions of temperature and pressure the solutions lie far from the hypercritical region where nonideality (and consequent nonlinearity) is expected.

Conclusion

Dynamic light scattering measurements have been reported as functions of concentration and temperature for toluene (a good solvent) and cyclohexane, methylcyclohexane, and deuterated methylcyclohexane (Θ solvents). In the good solvent region the logarithmic reduced DLS correlation length, ξ_h/r_h, decays for more than a decade logarithmically against MW weighted concentration according to an empirical scaling relation. However that simple correlation does not hold at small MW and/or low concentration. The bulk of the present results refer to low and intermediate M_w, while the overwhelming majority of literature data refer to high or even to very high M_w. From the present results it is seen that the universal behavior of the hydrodynamic correlation length referred to by Wiltzius, Cannell and

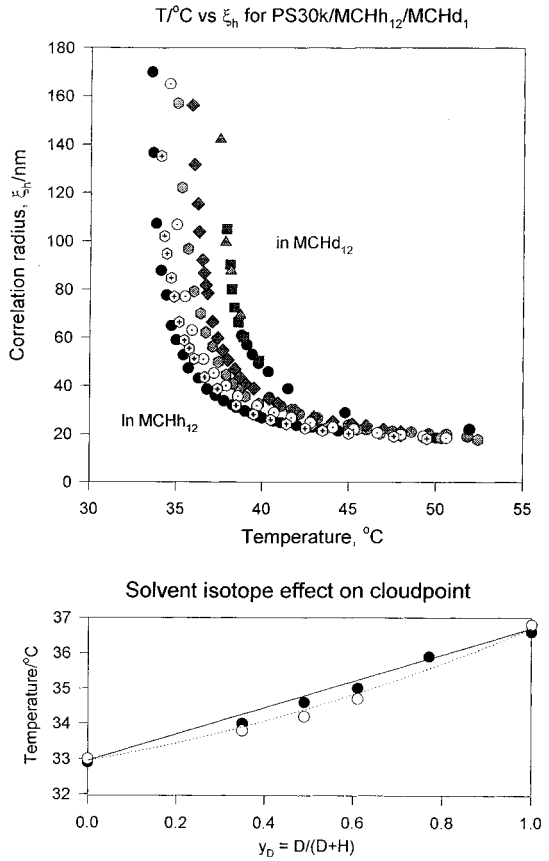

Figure 9. (a) Correlation radius as a function of temperature for a series of PS30k/MCHh$_{12}$/MCHd12 solutions (0.109 segment fraction): reading from left to right near the top of the figure, $y_D = 0.00$, 0.35, 0.49, 0.61, 0.77, and 1.00. The several different symbols in the $y_D = 1.00$ data refer to separate runs on different duplicate samples. (b) Cloud point temperature vs y_D for the series of solutions shown in part a. Solid points = visual cloud points. Open points = cloud points from empirically determined zeros of DLS diffusion constants. Height of data points corresponds to ±0.15 K.

Schaefer[3] is limited to very high M_w's, higher concentrations, and in the case of Θ solvents to temperatures well above T_Θ. Moreover, for polystyrenes at M_w's studied by us, criticality determines the behavior of the dynamic correlation lengths. Thus in the poor solvent region ξ_h diverges (increases) logarithmically as the transition temperature is approached at near critical concentration. In the present paper, that approach has been quantified for a series of cyclohexane, methylcyclohexane, and deuterated methylcyclohexane solutions, and the results have been compared with those for toluene using a reduced description of the data. The MCHh$_{12}$/MCHd$_{12}$ solvent isotope effect on demixing is small in this low-pressure part of the phase diagram (i.e., far from hypercritical conditions). We find [$(T_{cr,d} - T_{cr,h}) = 3.7 \pm 0.2$ K] and conclude that this solvent couple is nearly ideal.

Table 5. Solvent Isotope Effects in PS30k/MCHh$_{12}$/PS30k/MCHd$_{12}$ Solutions (0.109 Segment Fraction PS)

atom fraction of *D* in solvent hydrogen, [*D*/(*H* + *D*)]	visual cloud point (°C)	DLS diffusion determined cloud point (°C)
0.00	32.9	33.0
0.35	34.0	33.8
0.49	34.6	34.2
0.61	35.0	34.7
0.77	35.9	
1.00	36.6	36.8

Acknowledgment. This work was supported by the Division of Materials Sciences, U.S. Department of Energy.

References and Notes

(1) Berry, G. C. *Adv. Polym. Sci.* **1994**, *114*, 233.
(2) Brown, W.; Nicolai, T. In *Dynamic Light Scattering. The method and some applications*; Brown, W., Ed.; Clarendon Press: Oxford, England, 1993; Chapter 6, pp 272−318. Brown, W.; Nicolai, T. *Colloid Polym. Sci.* **1990**, *268*, 977.
(3) Wiltzius, P.; Haller, P. R.; Cannell, D. S.; Schaefer, D. W. *Phys. Rev. Lett.* **1983**, *51*, 1183.
(4) Fetters, L. J.; Hadjichristidis, N.; Lindner, J. S.; Mays, J. W. *J. Phys. Chem. Ref. Data* **1994**, *23*, 619.
(5) Schmidt, M.; Burchard, W. *Macromolecules* **1981**, *14*, 210.
(6) Szydlowski, J.; Van Hook, W. A. *Macromolecules* **1998**, *31*, 3266.
(7) Luszczyk, M.; Rebelo, L. P. N.; Van Hook, W. A. *Macromolecules* **1995**, *28*, 745.
(8) Imre, A.; Van Hook, W. A. *J. Phys. Chem. Ref. Data* **1996**, *25*, 637.
(9) Kratochvil, P. *Classical light scattering from polymer solutions*; Elsevier Press: Amsterdam, 1987.
(10) Szydlowski, J.; Van Hook, W. A. In preparation.
(11) Yaws, C. L., Ed. *Handbook of Viscosity*; Gulf Publ. Co.: Houston, TX, 1995.
(12) Lide, D. R., Ed. *Handbook of Chemistry and Physics*, 71st ed.; CRC Press: Boca Raton, FL, 1990.
(13) Sun, Z.; Wang, C. H. *Macromolecules* **1994**, *27*, 5667.
(14) Ilier, C.; Klein, H.; Woermann, D. *Macromolecules* **1995**, *28*, 1003.
(15) Melnichenko, Y. Personal communication.
(16) Higgins, J. S.; Benoit, H. C. *Polymers and Neutron Scattering*; Clarendon Press: Oxford, England, 1994.
(17) Singh, R. R.; Van Hook, W. A. *J. Chem. Phys.* **1987**, *87*, 6097.

MA971777O